Observations of entry and exit of Potential Vorticity at the sea surface

Arnaud Czaja and Ute Hausmann

Department of Physics, Imperial College, London [*]

October 16, 2008

_____

[*]Author address: Dr. A. Czaja, Imperial College, Prince Consort Road, Huxley Building, Room 726; London SW7 2AZ, UK. tel: +44 (0)20 7594 1789 fax: +44 (0)20 7594 7900 email: a.czaja@imperial.ac.uk

1

Abstract

Although potential vorticity (PV) is central to many theories of the oceanic circulation, the entry / exit of PV at the sea surface has not been thoroughly discussed from an observational perspective. After clarifying the notion of 'PV entry and exit', and the mechanisms responsible for it, we present a climatology of this quantity for the Northern Hemisphere.

It is found that surface PV loss over western boundary current regions and their interior extension is a robust feature over the North Pacific and Atlantic basins. At high latitudes, mechanical and diabatic effects act in concert in the North Atlantic to drive net PV exit. In the Pacific, however, these effects oppose each other and the net entry - exit of PV is more uncertain. At low latitudes, surface winds are found particularly important in setting surface PV exit in the Pacific, equatorward of the inter-tropical convergence zone.

1 Introduction

Potential vorticity (hereafter PV) is a central concept in physical oceanography. Observationalists use it frequently as a way to trace water masses (e.g., Talley and Mc Cartney, 1982); theoreticians put it at the core of our understanding of how the ocean is set into motion (e.g., Rhines and Young, 1982; Luyten et al., 1983). Surprisingly, however, and even though maps of potential vorticity have been frequently discussed (e.g., McDowell et al., 1982; Keffer, 1985; Talley, 1988; O'Dwyer and Williams, 1997), the sources and sinks of PV for the global ocean, and PV pathways from sources to sinks in the oceanic interior are not known from an observational perspective.

Traditionally, and this mostly reflects the theoretical work done with single or multi-layer quasigeostrophic models, anticyclonic windstress curl is thought of as a sink of PV, being balanced by frictional PV gain at the western boundary (e.g., Stommel, 1948) or surface PV gain due to cyclonic windstress curl over the subpolar gyre (e.g., Marshall, 1984). Surface cooling is also believed to be an important mechanism of PV loss (destruction of stratification) and, conversely, surface heating (creation of stratification) a mechanism of PV gain.

These mechanical and diabatic contributions to PV sources and sinks have been elegantly put together in a single framework through the concept of 'J-vectors', which represent the total (advective + non advective) transport of potential vorticity within the ocean (Haynes and McIntyre, 1987; 1989;

Marshall and Nurser, 1992; Marshall, 2000). Denoting the potential vorticity by Q (rigorous definitions are given below), the J-vector by $\boldsymbol{J}$, density by ρ and time by t, the conservation equation for PV can be written in flux form as,

$$\frac{\partial(\rho Q)}{\partial t} + \boldsymbol{\nabla} \cdot \boldsymbol{J} = 0 \tag{1}$$

A major implication of (1) is that, in steady state, $\boldsymbol{J}$ must be non divergent. In subtropical gyres, where Sverdrup dynamics predicts a downward advective transport in the interior of the ocean, one thus expects a surface entry of PV into the ocean. Conversely, over subpolar gyres, the Sverdrup upward advective transport must be matched by a surface PV exit out of the ocean! (Note that these simple predictions omit the effect of PV transport by eddy motions and, as a result, are only indicative of a possible dynamical regime).

It is our purpose to map from observations these surface entry / exit of PV, discuss their meaning and the mechanisms responsible for their existence (diabatic vs. mechanichal). To our knowledge, this has not yet been done from observations, even though the concept of J-vectors has been used to infer observational estimates of subduction rates over the North Atlantic (Marshall et al., 1993), the sea surface PV entry / exit computed from an ocean general circulation model of the North Atlantic (Marshall et al., 2001), eddy - driven PV input into the thermocline (Csanady and Vittal, 1996), the structure of the thermocline (Marshall, 2000), and, more recently, to discuss the role of winds in forming mode waters (Thomas, 2005).

The paper is structured as follows. We present in section 2 some background on potential vorticity and the J-vector framework. In particular, we wish to clarify the concept of surface PV entry and exit, that is, whether PV is actually exchanged between the atmosphere and ocean at the sea surface. In section 3, we present an observational estimate of the mechanical contribution to the air-sea PV flux, while a parallel effort is made in section 4 for the diabatic contribution. The net PV flux is discussed in section 5. A discussion and a conclusion section are offered in section 6 and 7, respectively.

2   Physics of J vectors

2.1   PV entry and exit at the sea surface

The framework for Ertel's potential vorticity (PV) transport in geophysical flows has been set out in various papers in both an oceanic and atmospheric context (Haynes and McIntyre, 1987; 1989; Hoskins, 1991; Marshall and Nurser, 1992; Csanady and Vittal, 1996; Marshall, 2000; Marshall et al., 2001). Following Marshall and Nurser (1992), we define the potential vorticity Q as

$$PV \equiv Q = -\frac{\boldsymbol{\xi} \cdot \boldsymbol{\nabla} \sigma}{\rho} \qquad (2)$$

in which ρ is seawater density, σ is the potential density (minus 1000 kgm^{-3}) and $\boldsymbol{\xi}$ is the absolute vorticity vector equal to the sum of the relative ($\boldsymbol{\zeta}$) and planetary ($2\boldsymbol{\Omega}$) vorticity vectors. The minus sign in (2) is introduced so that

PV is positive in the Northern Hemisphere in regions where isopycnals are flat (i.e., nearly horizontal). The unit of Q is $m^{-1}s^{-1}$ or, defining a unit of 'PV-substance' (pvs) as $1pvs = 1kgm^{-1}s^{-1}$, Q can be expressed in units of pvs/kg.

The flux of PV at a given position in space and time (in units of $pvs\ m^{-2}s^{-1}$), hereafter denoted as the J-vector, or simply $\boldsymbol{J}$, is given by (we refer the reader to the above literature for a derivation of this formulae),

$$\boldsymbol{J} = \rho Q \boldsymbol{u} + \boldsymbol{\xi}\frac{D\sigma}{Dt} + \boldsymbol{F} \times \boldsymbol{\nabla}\sigma \tag{3}$$

In eq. (3), $\boldsymbol{u} = (u\boldsymbol{i}, v\boldsymbol{j}, w\boldsymbol{k})$ denotes the three dimensional velocity field, $(\boldsymbol{i}, \boldsymbol{j}, \boldsymbol{k})$ being the local zonal, meridional and vertical unit vectors on the sphere and (u, v, w) the associated velocity components, $D\sigma/Dt$ is the lagrangian derivative of density, and $\boldsymbol{F}$ is the viscous body force per unit mass,

$$\boldsymbol{F} = \frac{D\boldsymbol{u}}{Dt} + 2\boldsymbol{\Omega} \times \boldsymbol{u} + \frac{1}{\rho}\boldsymbol{\nabla}p + g\boldsymbol{k} \tag{4}$$

p being the pressure and g gravity. The first term on the r.h.s of (3) represents the advective transport of PV while the two remaining terms are non advective and will be referred to in the following as the diabatic (involving exchange of heat and water at the air-sea interface and thereby leading to $D\sigma/Dt \neq 0$) and mechanical (involving viscous effects, $\boldsymbol{F} \neq \boldsymbol{0}$) components of the J-vector, respectively.

The flux of PV across the sea surface (hereafter denoted by J_s) is obtained by dotting (3) with the local ocean surface normal. Approximating the latter

by $\boldsymbol{k}$ and setting $w = 0$ at the sea surface ($z = 0$), we obtain

$$J_s = (\boldsymbol{\xi}\frac{D\sigma}{Dt} + \boldsymbol{F} \times \boldsymbol{\nabla}\sigma)_{z=0} \cdot \boldsymbol{k} \tag{5}$$

which, using further $\boldsymbol{\xi} \cdot \boldsymbol{k} \simeq f$ in which f is the Coriolis parameter (small Rossby number approximation), is rewritten as

$$J_s = f(\frac{D\sigma}{Dt})_{z=0} + (\boldsymbol{F} \times \boldsymbol{\nabla}\sigma)_{z=0} \cdot \boldsymbol{k} \tag{6}$$

Introducing further the mechanical and diabatic components,

$$J_s^{diab} = f(\frac{D\sigma}{Dt})_{z=0} \tag{7}$$

and

$$J_s^{mech} = (\boldsymbol{F} \times \boldsymbol{\nabla}\sigma)_{z=0} \cdot \boldsymbol{k} \tag{8}$$

we write

$$J_s = J_s^{diab} + J_s^{mech} \tag{9}$$

As emphasized in Rhines (1993) care must be taken when relating $D\sigma/Dt$ and $\boldsymbol{F}$ to air-sea buoyancy flux and surface windstress, respectively. Indeed, the terms in (6) represent vertical divergence of turbulent buoyancy and momentum transport, not the turbulent transport themselves. An assumption about the vertical structure of those fluxes in the mixed layer will have to be made in order to relate directly $D\sigma/Dt$ and $\boldsymbol{F}$ to surface buoyancy fluxes and windstress –see sections 3 and 4 below. Anticipating slightly on the result, we identify the diabatic component of J_s as reflecting the loss (gain) of stratification when there is surface buoyancy loss (gain) by the ocean.

Conversely, the mechanical component of J_s is interpreted as the loss (gain) of stratification associated with a dense-to-light (light-to-dense) Ekman drift –see Fig. 1.

2.2 Further background on J-vectors

Two results from the literature particularly help the analysis below. First, the "impermeability theorem" (Haynes and McIntyre, 1987). The latter states that the mass weighted PV content of any isopycnal layer can only be changed through fluxes where the layer intersects a boundary. Sea surface PV entry - exit is thus a component of the PV budget of isopycnal layers, the remaining terms of this budget involving frictional effects where the isopycnal layers intersect bathymetric features or the lateral boundaries of ocean basins (which we have not attempted to estimate in this study). For this reason, the global average of J_s does not need to be zero. Net PV gain or loss at the sea surface can be balanced by frictional sources and sinks at the basin boundaries or bottom.

Another important result is that of Schäar (1993), who showed that, irrespective of the nature of the PV transport (i.e., advective, frictionally or diabatically induced), it must be equal, in a statistically steady state to $\boldsymbol{J} = \boldsymbol{\nabla} B \times \boldsymbol{\nabla} \sigma$, in which B is the Bernoulli function. For typical ocean conditions (e.g., Marshall and Nurser, 1992) this reduces to $\boldsymbol{J} \simeq f \boldsymbol{u}_g \cdot \boldsymbol{\nabla} \sigma$, in which $\boldsymbol{u}_g$ is the geostrophic velocity. This relation thus allows a simple

interpretation of the net PV transport ($J_s^{mech} + J_s^{diab}$) as density gain following the geostrophic flow (PV exit) or density loss following the geostrophic flow (PV entry).

2.3 Is there air-sea exchange of PV between the ocean and the atmosphere?

The J-vector framework shows that there is, in general, a non zero PV flux at the air-sea interface. We wish to clarify here the physical meaning of this flux, and whether it can be thought of as an exchange of PV between the ocean and the atmosphere.

To do so, we consider a 'thought'-experiment akin to that of Rhines (1993), in which a rotating box is filled with two immiscible and (stably) stratified fluids (simply characterized by potential temperature θ) with no relative motion (Fig. 2). The upper fluid (loosely representing the atmosphere) is initially colder than the lower fluid (the ocean) fluid at the interface, and we let heat transfer and diffusive processes drive the system towards a state of uniform temperature distribution θ_{eq} (Fig. 2, dashed line). There is no exchange of heat with the surroundings as the box is assumed thermally insulated form the surroundings.

From the PV point of view, each fluid is going from a state of high PV (stratified) to a state of zero PV (no stratification at all), hence the J-vectors must be directed outward for both fluid (PV loss). The impermeability

theorem (section 2.2) is a powerful tool to analyze more precisely the sense of this PV transfer. Indeed, what happens is simply that each fluid "fills" with the intermediate temperature class θ_{eq}, and the PV contained in the warmer and colder layers is transported away from the central region with those layers, as indicated by the black arrows. Of importance here is the fact that the PV transport converges at the interface: the latter acts as a reservoir in which PV is accumulated in this thought-experiment.

This simple example shows that rather than being exchanged between ocean and atmosphere, like heat is (grey arrow in Fig. 2), PV transports converge (or diverge) at the air-sea interface. For this reason, we will hereafter use the 'PV entry/exit' rather than 'air-sea PV flux' terminology.

3 Wind contribution to PV entry and exit

3.1 Methodology

To start with, we rewrite the non conservative force $\boldsymbol{F}$ in (3) as,

$$\boldsymbol{F} \equiv \frac{1}{\rho_o} \frac{\partial \boldsymbol{\tau}}{\partial z} \qquad (10)$$

in which ρ_o is a reference density, and $\boldsymbol{\tau}$ is a turbulent stress representing the vertical transport of horizontal momentum by small scale processes. As emphasized in section 2.1 some assumption about the turbulent momentum fluxes must be made in order to relate the divergence of the latter to the surface windstress. Considering that the mixed layer depth h characterizes

the vertical scale of the layer experiencing significant turbulent momentum stresses, we assume $\partial \boldsymbol{\tau}/\partial z \simeq \boldsymbol{\tau}_s/h$, in which $\boldsymbol{\tau}_s = (\tau_x \boldsymbol{i}, \tau_y \boldsymbol{j})$ is the surface windstress vector. Assuming further that the density at the sea surface equals the mixed layer density σ_m,

$$\sigma_{z=0} \simeq \sigma_m \tag{11}$$

we finally compute the mechanical contribution to J_s as

$$J_s^{mech} \simeq (\frac{\boldsymbol{\tau}_s}{\rho_o h} \times \boldsymbol{\nabla}\sigma_m) \cdot \vec{k} \tag{12}$$

Equation (12) makes the link with Schär's formulation (section 2.1) particularly clear, with J_s^{mech} simply representing the density advection by the Ekman drift. This is one of term of the mixed layer density budget needed to balance, in the mean, the geostrophic advection of density. To put a number on this relationship, a stress $\tau_x = 0.1 N m^{-2}$ acting on mixed layer density gradient $\partial\sigma_m/\partial y = 1 kg \ m^{-3}/1000 km$ and a mixed layer depth $h = 100m$ leads to $J_s^{mech} \simeq 10^{-12} pvs \ m^{-2}s^{-1}$. As we will see, this number is typical of observed entry/exit of PV at the sea surface.

In order to compute (12) a monthly windstress climatology was constructed over the 1960-1987 period from the NCEP-NCAR reanalysis (Kalnay et al., 1996). The global monthly mixed layer depth climatology of Montégut et al. (2004) was used to estimate h (temperature criterion). The mixed layer density was computed by averaging potential density from the World Ocean Atlas (Konkright et al, 2002) over the mixed layer. All PV flux calculations shown in this paper were carried out with monthly climatologies on a $2° \times 2°$

degrees longitude-latitude grid.

3.2 Northern Hemisphere maps

We first estimate, at a given location, the long term mean value of J_s^{mech} by annually averaging (12) at each oceanic gridpoint (Fig. 3). Entry of PV (light shading) is seen in a large latitudinal band stretching from about $30°$ to $\simeq 5-10°$. Exit of PV (dark shading) is seen poleward and equatorward of this band. Unlike for quasi-geostrophic PV, the line separating mechanical PV entry and exit does not coincide with the zero windstress curl line. Indeed, because of the larger zonal than meridional winds, and the larger meridional than zonal density gradients, the map in Fig. 3 is dominated by $J_s^{mech} \simeq \tau_x \partial \sigma_m / \partial y \rho_o h$, and so vanishes wherever τ_x or $\partial \sigma_m / \partial y$ does. A simplified calculation of (12) in which τ_y is set to zero illustrates this result (Fig. 4a, to be compared with Fig. 3). Only over coastal areas such as the western North Atlantic, the Eastern North Pacific and the western Indian coastline is the signature of meridional stress acting on zonal density gradients seen.

This simplified calculation has interesting features, such as significant departures from latitude circles. We have thus decomposed it further and show in Fig. 4b the result of a calculation in which the meridional density gradient is set to a constant value everywhere. The zero line of the resulting map is thus solely attributable to the vanishing of the zonal windstress and as a result runs approximately along $30°N$. Comparison of Fig. 4a and

Fig. 4b indicates that extrema in σ_m have a profound effect on J_s^{mech}. At low latitudes, one observes in Fig. 4a a tongue of upward PV fluxes (dark shading) reflecting the density extrema associated with the Inter-Tropical Convergence Zone (ITCZ – i.e., a region where density decreases, rather than increases, poleward) which is not seen in Fig. 4b. Local variations in density gradient are also important over the (Eastern) Indian Ocean and the western North Atlantic, where they are instrumental in establishing a pattern of PV entry on the poleward flank of the separated Gulf Stream, and intensified PV exit over the Labrador current.

As mentionned above, these patterns can simply be understood from the direction of the Ekman drift. The upper ocean experiences a loss of stratification (PV exit) when the Ekman drift is directed from dense to light and, conversely, it experiences a gain of stratification (PV entry) when the Ekman drift is directed from light to dense.

3.3   Isopycnal analysis

An alternative way to discuss the PV entry / exit at the sea surface is to consider how it affects isopycnal layers, rather than geographical locations (section 2.2 and "the impermeability theorem"). We have indicated in Figs. 3 and 4 the annual mean position of some selected isopycnal outcrops (thin black lines). The latter actually move significantly meridionally and zonally throughout the year (Fig. 5) so that a proper isopycnal analysis must track

the outcrop lines through their seasonal migration. We have thus followed a range of isopycnal layers (density $[\sigma_m, \sigma_m + \Delta\sigma_m]$ with $\Delta\sigma_m = 0.2 kgm^{-3}$) and display in Fig. 6a how much PV enters / leaves each layer per unit time, i.e., we plot

$$\Delta J_s^{mech}(\sigma_m, t) = \frac{1}{\Delta\sigma_m} \int_{\sigma_m}^{\sigma_m + \Delta\sigma_m} J_s^{mech}(x, y, t) dx dy \qquad (13)$$

in which t is a given calendar month. Strikingly, only a weak seasonal cycle is seen, most isopycnals experiencing PV exchange of only one sign throughout the year. The $\sigma_m \simeq 24.5 kgm^{-3}$ separates those isopycnal layers experiencing PV entry (lighter isopycnals) from those experiencing PV exit (denser isopycnals). This reflects the belt of surface westerlies poleward of the average position of the $\simeq 24.5 kgm^{-3}$, destratifying the surface by advecting dense water equatorward, and, conversely, Trade winds equatorward of this isopycnal layer outcrop, stratifying the surface by advecting light water poleward (Fig. 1). Note that this simple dipolar pattern masks a significant compensation between PV entry and exit for light (low latitudes) isopycnals, as hinted at in Fig. 3 (e.g., the annual mean outcrop of $\sigma_m = 22$ –thin black line– experiences both PV entry and exit).

We display the annual mean of ΔJ_s^{mech} for the North Pacific (continuous) and North Atlantic (dashed) basins [1] separately in Fig. 6b. As expected from the higher surface density in the North Atlantic, the dipolar curve is shifted towards the right in the North Atlantic compared to the North Pacific

---

[1]The 'North Pacific' calculation also includes the Northern Indian ocean.

by about $1 kg\ m^{-3}$. Larger PV exit and entry is seen in the Pacific as a result of the larger size of this basin.

4   Diabatic contribution to PV input and exit

4.1   Methodology

Equation (7) shows that the diabatic component of the air-sea PV flux is proportional to $D\sigma/Dt$ estimated at the sea surface. Using the approximation (11), a slab mixed layer model can be used to compute $D\sigma/Dt_{z=0}$, with several terms making up the density tendency: air-sea buoyancy flux ($D_{air-sea}$, positive when buoyancy loss), entrainment of denser water from below the mixed layer (D_{ent}), mesoscale eddy density flux convergence D_{eddy} (e.g., Kraus-Turner, 1967; Large and Nurser, 2001),

$$h\frac{D\sigma_m}{Dt} = D_{air-sea} + D_{ent} + D_{eddy} \tag{14}$$

Using (7) and (11), we can then write,

$$J_s^{diab} = \frac{f D_{air-sea}}{h} + \frac{f D_{ent}}{h} + \frac{f D_{eddy}}{h} \tag{15}$$

To put numbers on this formula, a typical cooling of $100 W m^{-2}$ acting on a mixed layer of depth $h = 100m$ in midlatitudes ($f = 10^{-4}\ s^{-1}$) leads to a PV exit of $J_s^{diab} \simeq 2 \times 10^{-12}\ pvs\ m^{-2}s^{-1}$.

The challenge posed by estimating J_s^{diab} becomes readily apparent: neither the air-sea buoyancy flux, nor the entrainment or the lateral eddy flux

contribution to the buoyancy budget are known precisely from observations. We have nevertheless constructed a tentative estimate of the first two terms in (15), with no attempts at estimating the impact of the eddies, i.e., we will use

$$J_s^{diab} \simeq \underbrace{\frac{fD_{air-sea}}{h}}_{J_s^{(diab,ao)}} + \underbrace{\frac{fD_{ent}}{h}}_{J_s^{(diab,ent)}} \tag{16}$$

The contribution $J_s^{(diab,ao)}$ from the air-sea buoyancy flux was estimated using the same mixed layer depth climatology as in section 3, plus a climatology of air-sea density flux developed recently at Imperial College (Howe and Czaja, 2008). The latter's thermal component is the adjusted climatology of Grist and Josey (2003) while, for the haline part, the evaporation from Grist and Josey (2003) and the precipitation from Xie and Arkin (1997) are used. Note that both the haline and thermal components are constrained to satisfy the global heat and freshwater budget obtained during WOCE (Ganachaud and Wunsch, 2001). We refer to the paper by Howe and Czaja (2008) for more discussion of this dataset.

The contribution $J_s^{(diab,ent)}$ is more problematic and we have simply aimed at giving a bound on the effects of entrainments. To get some insight into the latter, consider the following "thought-experiment". Consider an hypothetical ocean only subject to spatially uniform, seasonally varying, buoyancy forcing. Assume further that the net surface buoyancy flux is zero, with wintertime buoyancy loss balancing exactly summertime buoyancy gain, and let us consider the simplest case of uniform rotation ($f = constant$). Because of

the seasonal correlation between $D_{air-sea}$ and h (summertime air-sea buoy-
ancy gain when the mixed layer is shallow, buoyancy loss when the mixed
layer is deep), there will be a net annual gain of PV by the ocean. This is
problematic because, in this thought-experiment, there is no oceanic circula-
tion to transport PV to lateral boundaries where a frictional PV flux could
balance the surface PV input (or to a region of surface PV loss, if it was
present). The reason is simple: in wintertime, cooling of the mixed layer
occurs not only at the sea surface but also at the mixed layer base through
entrainment of cold water from below. This additional cooling mechanism
will, in this thought experiment, compensate exactly the larger summertime
PV gain caused by the shallowing of the mixed layer. As a way to estimate
this effect we have computed $J_s^{(diab,ent)}$ using standard slab mixed layer model
results for D_{ent} (e.g., Kraus and Turner, 1967),

$$D_{ent} = w_{ent}(\sigma_{ent} - \sigma_m) \tag{17}$$

in which σ_{ent} is the density of water that is entrained into the mixed layer
and w_{ent} is the entrainment velocity,

$$w_{ent} = \begin{cases} 0 & \text{when } \frac{\partial h}{\partial t} \leq 0 \\ \partial h/\partial t & \text{when } \frac{\partial h}{\partial t} > 0 \end{cases} \tag{18}$$

Note that equation (18) omits the contribution to entrainment resulting from
convergence / divergence of the flow, but it allows for a simple calculation
using the mixed layer depth climatology mentionned above. The density

difference appearing in (17), namely,

$$\Delta_{ent}\sigma \equiv \sigma_{ent} - \sigma_m \qquad (19)$$

is taken as a constant parameter. In their attempt at estimating the effects

of entrainment on transformation rates, Garrett and Tandon (1997) typically

used a value of $\Delta_{ent}b = 10^{-3}\ ms^{-2}$ for the buoyancy jump at the base of the

mixed layer, i.e., $\Delta_{ent}\sigma = \rho_o\Delta_{ent}b/g \simeq 0.1\ kgm^{-3}$. Considering that our

estimate of w_{ent} is certainly underestimated by the use of a smooth monthly

climatology of mixed layer depth, we have opted for investigating a range of

values $0 \leq \Delta_{ent}\sigma \leq 0.5\ kgm^{-3}$.

4.2 Northern Hemisphere maps

The annual mean value of J_s^{diab} computed with a value $\Delta_{ent}\sigma = 0.5\ kgm^{-3}$ is

plotted for the Northern Hemisphere in Fig. 7, in a format analog to Fig. 3.

PV exit (dark shading) over the Gulf Stream and the Kuroshio is pronounced,

reflecting the large wintertime buoyancy loss over these regions. PV exit is

also found on the eastern side of Atlantic and Pacific subtropical basins,

reflecting the large surface evaporation maintained by the slow descent of

dry air over the oceans in the subsidence branch of the Hadley - Walker

circulations. At high latitudes, PV exit is found over the subpolar North

Atlantic but not over the subpolar North Pacific, which experiences PV entry.

The result of a calculation in which entrainment effects are not considered

($\Delta_{ent}\sigma = 0$) is shown in Fig. 8a. Compared to Fig. 7, regions of PV exit

become less extensive, disappearing almost entirely in the subpolar North Atlantic. This is consistent with the above 'thought-experiment', the seasonal correlation between $D_{air-sea}$ and h biasing $J_s^{(diab,ao)}$ towards its summertime value, when heating of the ocean leads to PV entry. To emphasize this point, we have repeated the calculation in Fig. 8a using annual mean mixed layer depth, rather than seasonal values (Fig. 8b). PV exit is then found over most of the North Atlantic and North Pacific, the maps simply reflecting the annual mean value of $D_{air-sea}$.

The fact that the subpolar North Pacific experiences diabatic PV entry results from the net surface buoyancy gain of this basin, itself reflecting the weak surface evaporation associated with cold North Pacific sea surface temperature (e.g., Warren, 1983). Very large entrainment effects would be required to bring J_s^{diab} to zero (this happens when $\Delta_{ent}\sigma > 1.25 \ kgm^{-3}$), which seems unrealistic. It is of course possible that the surface buoyancy gain is overestimated over the subpolar gyre, so that the numbers are overall uncertain (note however that, as discussed in Howe and Czaja (2008), our $D_{air-sea}$ dataset is in good agreement with others over this region). Nevertheless, Figs. 7 and 3 highlight a very interesting qualitative difference between North Atlantic and Pacific subpolar basins. In the North Atlantic, both mechanical and diabatic contributions set a pattern of surface PV exit. In the North Pacific, however, mechanical and diabatic effects oppose each other with the winds driving PV exit but diabatic effects PV entry.

4.3   Isopycnal analysis

Figure 9a displays the seasonal evolution of the diabatic component of PV entry/exit computed using a value $\Delta_{ent}\sigma = 0.5\ kgm^{-3}$, for the same isopycnal layers as in section 3, i.e. a plot of,

$$\Delta J_s^{diab}(\sigma_m, t) = \frac{1}{\Delta\sigma_m}\int_{\sigma_m}^{\sigma_m+\Delta\sigma_m}(J_s^{(diab,ao)} + J_s^{(diab,ent)})dxdy \qquad (20)$$

as a function of calendar months and isopycnal layers. The striking difference with ΔJ_s^{mech} (Fig. 6a) is the strong seasonal cycle. In winter, surface cooling leads to PV exit but the reverse occurs in summer, despite the isopycnal layers typically moving poleward at that time of year (Fig. 5). Thus, rather than experiencing solely PV input or exit throughout the year (as J_s^{mech} does), diabatic effects drive alternate, seasonally changing, PV entry/exit in isopycnal layers. The summertime PV input is expected from the high values of PV observed in oceanic seasonal thermoclines (e.g., Talley, 1988; Csanady and Vittal, 1996). Conversely, wintertime surface PV exit is consistent with the presence of low PV in deep mixed layers (Talley and Mc Cartney, 1982; Thomas, 2005).

Comparison of Fig. 6a and 9a suggests that, on a given month, PV entry/exit is dominated by the diabatic contribution (note the larger contour interval in Fig. 9a compared to Fig. 6a). Owing to the strong cancellation between summer and winter, however, the annual mean of ΔJ_s^{diab} is comparable, although still larger on average, than that for ΔJ_s^{mech} (Fig. 9b). The North Atlantic (dashed) displays PV exit over almost all isopycnal layers

while the North Pacific shows a more complicated structure. PV input is found over $\sigma_m \simeq 25$, corresponding to isopycnals whose mean outcrop position is in the subpolar gyre (Fig. 7, thin black line labelled 25), but is even larger over the light isopycnals making the rim of the Indo-Pacific 'warm pool' ($\sigma_m \simeq 22$). PV exit is only hinted at for the densest layers outcropping in winter ($\sigma_m > 26$ –see Fig. 5).

5   Net surface PV entry / exit

5.1   Northern Hemisphere maps

The net PV entry/exit at the sea surface is estimated as

$$J_s = J_s^{diab,ao} + J_s^{diab,ent} + J_s^{mech} \tag{21}$$

and its annual mean distribution is shown in Fig. 10, in a format similar to Fig. 3. A value $\Delta_{ent}\sigma = 0.5\ kgm^{-3}$ was used, so that the estimate in Fig. 10 is the sum of those shown in Fig. 3 and Fig. 7. To gain some confidence in the pattern, we compare it to Marshall et al. (2001)'s Fig. 4c, which shows, for the North Atlantic only, an ocean model estimate of J_s. The comparison is very good, both in sign and amplitude (the comparison obviously depends upon the choice of $\Delta_{ent}\sigma$ and we have not attempted to optimize this parameter to improve the comparison with Marshall et al's map). The North Atlantic shows a quadrupolar pattern of air-sea PV flux, with PV gain at low latitudes, PV loss in the eastern subtropics and over

the Florida current, PV gain south of the separated Gulf Stream and over the Labrador current, and PV loss along the Gulf Stream and over most of the subpolar gyre. The strongest PV loss is found over the Gulf Stream, with values larger than 10.10^{12} pvs m^{-2} s^{-1} (see scalings in sections 3 and 4). Considering the uncertainties in the observational datasets needed to estimate J_s, and the simplicity of our model for entraiment, the comparison is very encouraging.

The Northern Hemisphere map (Fig. 10) as a whole shows striking differences between the Atlantic and Pacific. In the extra-tropics, the tongue of PV exit over the western boundary current is limited to about $40°N$ and mid-basin ($\simeq 180°W$) in the North Pacific wheareas it extends all the way to the high latitudes in the North Atlantic. Put differently, the net subpolar PV entry, which is limited to the Labrador current area in the Atlantic, is seen to occupy the whole subpolar gyre in the North Pacific. The opposition between mechanical and diabatic effects in the North Pacific, but their constructive association in the North Atlantic (see section 4), is clearly key to establishing this contrast between the basins.

5.2   Isopycnal analysis

Figure 10 suggests that isopycnals outcropping frequently over the North Pacific subpolar gyre should experience net PV entry. To check this we turn to a proper isopycnal analysis for J_s and first identify the isopycnals

layers experiencing Ekman downwelling (hereafter "subtropical isopycnals")
or upwelling (hereafter "subpolar isopycnals") in the annual mean (Fig. 11
-for this purpose the same monthly windstress climatology was used as in
section 3). In the North Atlantic (dashed line), isopycnals denser than $\sigma_m \simeq$
27) experience Ekman suction (Ekman velocity $w_{Ek} > 0$) while those lighter,
pumping ($w_{Ek} < 0$). The situation in the North Pacific (continuous line)
is a bit more complicated, with suction at $\sigma_m > 25.5$ and $\sigma_m < 21.75$ and
pumping in between.

Next we display in Fig. 12 the result of a calculation similar to Figs. 4b,
9b but for J_s rather than J_s^{mech} and J_s^{diab}. In the North Pacific (continuous
curve) a more intuitive PV exit rather than input at high density ($\sigma_m >$
26) is now found, reflecting the fact that the densest "subpolar isopycnals"
only outcrop at the sea surface in winter, when the mixed layer experiences
buoyancy loss. The high latitude net PV input, so prominent in Fig. 10, is
still seen over the intermediate density range $\sigma_m \simeq 24 - 26$, but inspection of
Fig. 11 shows that the maximum PV entry at $\sigma_m \simeq 25.5$ in Fig. 12 coincides
with the subtropical / subpolar gyre boundary. Thus, the 'fixed location
analysis' (Fig. 10) somewhat distorts the isopycnal view (only light subpolar
gyre isopycnals experience net PV entry in the North Pacific). Additional
analysis of the role of heating and freshening in providing the buoyancy gain
for those 'inter-gyre isopycnals' indicate the freshening to be dominant (not
shown). This result is consistent with the presence of net precipitation at the

boundary between the gyres in the North Pacific as a result of the Summer Asian Monsoon (Czaja, 2008 –see his Fig. 3b).

A similar isopycnal analysis for the North Atlantic (Fig. 12, dashed curve) reveals a much simpler dipolar picture, with net PV exit for isopycnals denser than $\sigma_m \simeq 25$ and net PV entry for isopycnals lighter than $\sigma_m \simeq 25$. In other words, unlike in the North Pacific, there is no indication of an 'intermediate' (at the boundary between subpolar and subtropical gyres) isopycnal range experiencing net PV entry. Net PV exit is associated, on the lighter end ($\sigma_m \simeq 25 - 27$), with isopycnals outcropping in the subtropics in regions of Ekman downwelling, and experiencing PV loss associated with large scale subtropical evaporation and air-sea interactions over the Gulf Stream. On the denser end ($\sigma_m > 27$), net PV exit is associated with high latitude cooling and Ekman upwelling. Net PV input is solely confined to regions of Ekman downwelling. The broad peak in net PV exit at $\sigma_m \simeq 26 - 27$ is consistent with Marshall et al. (2001)'s isopycnal analysis for the North Atlantic (their Fig. 8), but their model study suggests net PV exit for all density classes, not solely for $\sigma_m \geq 25$ as found here.

6   Discussion

The estimates of surface PV entry / exit presented in this study must be taken with caution considering the large number of datasets which are needed to construct them: surface windstress, mixed layer depth and density, net sur-

face buoyancy and entrainment fluxes. It is hard to argue that the latter are known accurately and so are, consequently, our PV flux maps. A possible alternative, which we tried, is to use Schär (1993)'s formulation of the J-vector, which only requires knowledge of mixed layer density and surface pressure [2] –see section 2.2. In practise however, this method turned out to be difficult to use. Indeed, to obtain a global seasonal climatology of surface pressure, we used the sea surface height measurements from the Topex-Poseidon / Jason altimeters. Owing to errors on the geoid at the gridpoint scale ($2° \times 2°$), residual oceanic variability (a 12-yr mean was used which is short for proper ocean statistics) and errors on the hydrography (seasonal cycle of mixed layer density), the calculation turned out to be very noisy (and this in addition to the fact that Schär's formula itself is noisy by nature, since it is the advection of density by the geostrophic flow, i.e. a cross product of two gradient vectors).

Our assumptions for the distribution of turbulent fluxes in the mixed layer and our model for entrainment are admittedly crude. They do not take into account mixed layer entrainment of momentum, or the high frequency (synoptic) storm variability, or spatial variability of the density jump at the base of the mixed layer ($\Delta_{ent}\sigma$). We found however our main conclusions to be unchanged when varying $\Delta_{ent}\sigma$. The North Atlantic systematically

---

[2]At the sea surface, Schäar's expression reads $J_s = (\boldsymbol{\nabla} g\eta \times \boldsymbol{\nabla} \sigma_m).\boldsymbol{k}$ in which we have approximated the Bernoulli function by the surface geopotential height ($B = \frac{1}{2}|\vec{u}|^2 + p/\rho_o \simeq p/\rho_o = g\eta$, g being gravity and η the height of the sea surface).

displays net PV exit at high density and net PV entry at lower density, the value of $\Delta_{ent}\sigma$ solely changing the density at which the transition occurs and the overall magnitude of the PV exit / entry. In the North Pacific, a value $\Delta_{ent}\sigma \simeq 1 \ kgm^{-3}$ is needed to remove the net PV entry in intermediate density class seen in Fig. 12 ($\sigma_m = 24 - 26$), which seems unrealistic.

Probably the most striking result of our analysis is the difference between the distribution of PV entry / exit for the high latitude North Atlantic and Pacific. Because of the large poleward flow of warm waters associated with the thermohaline circulation in the Atlantic, there is a strong surface evaporative cooling at high latitudes which acts to remove PV at the sea surface. The westerlies add constructively to this, resulting, overall, in a net PV exit along the path of the North Atlantic Drift (Fig. 10) or isopycnal layers denser than $\sigma_m \geq 26$ (Fig. 12). In the subpolar gyre of the North Pacific, however, no such poleward circulation is found in upper layers and there is net surface buoyancy gain at high latitudes. Diabatic effects thus tend to restratify the surface (PV entry) and oppose the effect of the westerlies (PV exit) in the North Pacific. Our analysis suggests that, in total, diabatic effects dominate, with a net PV entry over the subpolar gyre (Fig. 10). This view is somewhat distorted from that seen in the isopycnal analysis of Fig. 12 (the bulk of the PV entry is experienced by 'inter-gyre isopycnals', the denser layers experiencing PV exit –see section 5.2).

Considering the uncertainties discussed above in the calculation of J_s,

it is difficult to claim with confidence that the North Pacific subpolar gyre experiences net surface PV entry. The compensation between diabatic and mechanical effects is appealing and might indeed lead to a neutral distribution of PV entry / exit for this region, i.e., $J_s \simeq 0$. Non eddying models of the subpolar gyre show indeed a scenario whereby, in the interior, advective PV transport balances frictional PV transport, thereby having no difficulty at dealing with a zero sea surface PV exit (Marshall, 2000). Alternatively, eddies acting downgradient on large isopycnic gradients of PV in the spring / early summer (e.g., Talley, 1985) could be instrumental in transporting into the oceanic interior the PV that enters through the sea surface, dominating over the upward mean PV transport by the Sverdrup flow (Fig. 13a). This is in sharp contrast with the dynamics suggested in the North Atlantic, in which a clear net PV exit is found at the sea surface, connecting to the mean upward PV transport by the Gulf Stream and the North Atlantic Drift ("thermohaline circulation") in the interior (Fig. 13b).

Some support for this view of the North Pacific is provided by the observed Tritium distribution (Fine et al., 1981). Indeed, considering that all the PV transport below the mixed layer is advective, a southward PV transport as in Fig. 13a should relate to a southward tracer transport. Fine et al. (1981) consistently show a significant southward spreading of high Tritium value towards the South for isopycnals outcropping in winter in the subpolar gyre ($\sigma_\theta = 26.02$, their Fig. 6). We note further that the state of affair de-

picted in Fig. 13a for the North Pacific is reminiscent of the dynamics at high latitudes of the Southern Ocean. There, downgradient eddy PV fluxes along isopycnal surfaces (i.e., downward and equatorward PV transport) have been suggested to drive the lower branch of the Deacon cell (Speer et al., 2000).

7   Conclusion

We have presented, for the first time, an observational estimate of PV entry/exit at the sea surface. The North Atlantic appears as a 'textbook' example of surface PV exit in the western boundary current extension / subpolar gyre and surface PV entry over most parts of the subtropical gyre, but investigation of the mechanisms setting this pattern highlight the complementary role of diabatic and mechanical processes. The North Pacific displays a more complicated pattern of PV entry / exit. Our main results can be summarized as follows:

- Air-sea buoyancy fluxes drive seasonally varying PV entry/exit on isopycnal layers whereas the winds do not.

- Western boundary currents and their interior extension experience net surface PV exit.

- Subtropical gyres experience both PV entry and exit, with similar patterns in the Atlantic and Pacific.

- The subpolar gyres of the North Pacific and Atlantic differ strikingly

in their surface distribution of PV exit and entry. This reflects the constructive effect of mechanical and diabatic effects in the North Atlantic, leading to a clear net PV exit along the path of the North Atlantic current, but their opposition in the North Pacific, leading to a more uncertain (possibly net entry) surface PV flux.

Our study illustrates the fundamentally coupled (ocean-atmosphere) nature of the entry and exit of PV at the sea surface. This is vividly illustrated in the tropical Pacific, where coupled air-sea interactions displace the ITCZ and its belt of warm water north of the equator, setting reversals in the meridional density gradient and surface PV exit equatorward of the ITCZ but PV entry on the poleward side of the ITCZ . Conversely, the presence of an active thermohaline cell in the Atlantic, leading to warmer sea surface temperature and evaporation at high latitudes in this basin compared to the North Pacific, is vividly 'seen' in the extension to high latitudes of the western boundary tongue of surface PV exit.

Clearly though, considering the large number of observational datasets needed to produce the air-sea PV flux, and the imperfections associated with them, further work with oceanic reanalyses, ocean-only GCMs or coupled ocean-atmosphere GCMs is needed to test the reproducibility of our results. It will be fascinating to match the surface PV entry / exit presented in this study with interior transport using eddy resolving GCM simulations.

References

Csanady, G. T., and G. Vittal, 1996: Vorticity balance of outcropping isopy-cnals, J. Phys. Oce., 26, 1952-1956.

Czaja, A, 2008: Atmospheric control on the thermohaline circulation, J. Phys. Oce., in press.

Fine, R. A., J. L. reid, H. G. Östlund, 1981: Circulation of Tritium in the Pacific Ocean, J. Phys. Oce., 11, 3-14.

Ganachaud, A. and C. Wunsch, 2003: Large-scale ocean heat and freshwater transports during the World Ocean Circulation Experiment, J. Clim., 16, 696-705.

Garrett, C., and A. Tandon, 1997: The effects on water mass formation of surface mixed layer time dependence and entrainment fluxes, Deep-Sea Res., 44, No 12, 1991-2006.

Gill, A. E. J., 1982: Atmosphere - Ocean Dynamics, Academic press.

Grist, J. P., and S. A. Josey, 2003: Inverse analysis adjustment of the SOC air-sea flux climatology using ocean heat transport constraints, J. Clim., 16, 3274-3295.

Haynes, P. H., and M. E. McIntyre, 1987: On the evolution of vorticity and potential vorticity in the presence of diabatic heating and frictional or other forces, J. Atm. Sci., 44, 5, 828-841.

Haynes, P. H., and M. E. McIntyre, 1990: On the conservation and imper-meability theorems for potential vorticity, J. Atm. Sci., 47, 16, 2021-2031.

Hoskins, B. J., 1991: Towards a PV-θ view of the general circulation, Tellus, 43AB, 27-35.

Howe, N. and A. Czaja, 2008: A globally balanced air-sea density flux clima-tology and global surface transformation rates, submitted to J. Phys. Oce.

Keffer, T., 1985: The ventilation of the world's oceans: maps of the potential vorticity field, J. Phys. Oce., 15, 509-523.

King, C., D. Stammer, and C. Wunsch, 1994: The CMPO/MIT Topex/Poseidon Altimetric data set, M.I.T, Centre for Global Change Sci-ence, Report No 30.

Kraus, E. B., and J. S. Turner, 1967. A one - dimensional model of the seasonal thermocline, II, Tellus, 19, 98-106.

Large, W. G., and A. J. G. Nurser, 2001: Ocean surface water mass trans-formation, Chap. 5.1 in 'Ocean Circulation and Climate', Academic Press, 715pp.

Luyten, J. R., J. Pedlosky and H. Stommel, 1983: The ventilated thermo-cline, J. Phys. Oce., 13, 292-309.

Marshall, D. P., 2000: Vertical fluxes of potential vorticity and the structure of thermocline, J. Phys. Oce., 30, 3102-3112.

Marshall, J. C., 1984: Eddy-mean flow interaction in a barotropic ocean model, Q. J. Roy. Met. Soc., 110, 573-590.

Marshall, J. C., and A. J. G. Nurser, 1992: Fluid dynamics of oceanic thermocline ventilation, J. Phys. Oce., 22, 583-595.

Marshall, J., A. J. G. Nurser, and R. G. Williams, 1993: Inferring the subduction rate and period over theh North Atlantic, J. Phys. Oce., 23, 1315-1329.

Marshall, J. C., D. Jamous, and J. Nilsson, 2001: Entry, flux, and exit of potential vorticity in ocean circulation, J. Phys. Oce., 31, 777-789.

McDowell, S., P. Rhines, and T. Keffer, 1982: North Atlantic potential vorticity and its relation to the general circulation, J. Phys. Oce., 12, 1417-1436.

O'Dwyer, J., and R. G. Williams, 1997: The climatological distribution of potential vorticity over the abyssal ocean, J. Phys. Oce., 27, 2488-2506.

Pedlosky, J., 1998. Ocean Circulation Theory, Springer, 453pp.

Rhines, P. B. 1993: Oceanic general circulation: wave and advection dynamics, NATO ASI series vol I 11, Modelling Oceanic Climate Interactions, D. Anderson and J. Willebrandt, eds.

Rhines, P. B. and W. R. Young, 1982: A theory of the wind driven circulation. I. Mid-ocean gyres, J. Mar. Res., 40, 559-596.

Schär, C., 1993: A generalisation of Bernoulli's theorem, J. Atm. Sci., 50, 1437-1443.

Schmitz, W. J., 1996. On the world ocean circulation: Vol II, The Pacific nd indian Oceans / a global update, Woods Hole Oceanographic Institution, Technical Report, WHOI-96-08.

Speer, K., S. R. Rintoul, and B. Sloyan, 2000: The diabatic Deacon cell, J. Phys. Oce., 3212-3222.

Talley, L. D., 1988: Potential vorticity distribution in the North Pacific, J. Phys. Oce., 18, 89-106.

Talley, L. D. and M. S. McCartney, 1982: Distribution and circulation of Labrador sea water, J. Phys. Oce., 12, 1189-1205.

Thomas, L., 2005: Destruction of potential vorticity by winds, J. Phys. Oce., 35, 2457-2466.

Warren B. A., 1983: Why is no deep water formed in the North Pacific?, J. Mar. Res., 41, 327-347.

Xie, P. P. and P. A. Arkin, 1996: Analyses of global monthly precipitation using gauge observations, satellite estimates, and numerical model predictions, J. Clim., 9, 840-858.

List of Figures

Figure 1: Schematic of the PV exit (entry) at an outcropping isopycnal surface associated with a surface westerly (easterly) stress and surface buoyancy loss (gain), assuming a simple equator-to-pole gradient of surface density. The PV flux (upward for PV exit, $J_s > 0$) is schematized as the white arrow.

Figure 2: A "thought-experiment" to illustrate the difference between the transfer of heat (left side, as indicated by the grey arrow) and PV (right side, black arrows). The initial potential temperature distributions are indicated by the continuous black lines while the dashed line defines the equilibrium temperature θ_{eq}. See text for details.
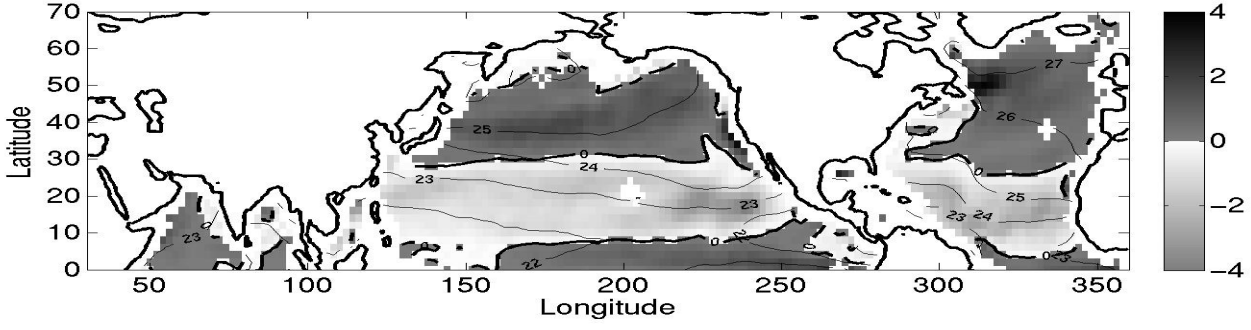
Figure 3: Annual mean mechanical contribution (J_s^{mech}) to the sea surface PV entry/exit (shading, dark when out of the ocean, light when into the ocean, in units of $10^{-12} pvs\ s^{-1} m^{-2}$, zero contour as black thick line) superimposed on annual mean mixed layer density (contoured every 1 kgm^{-3} in thin black lines).
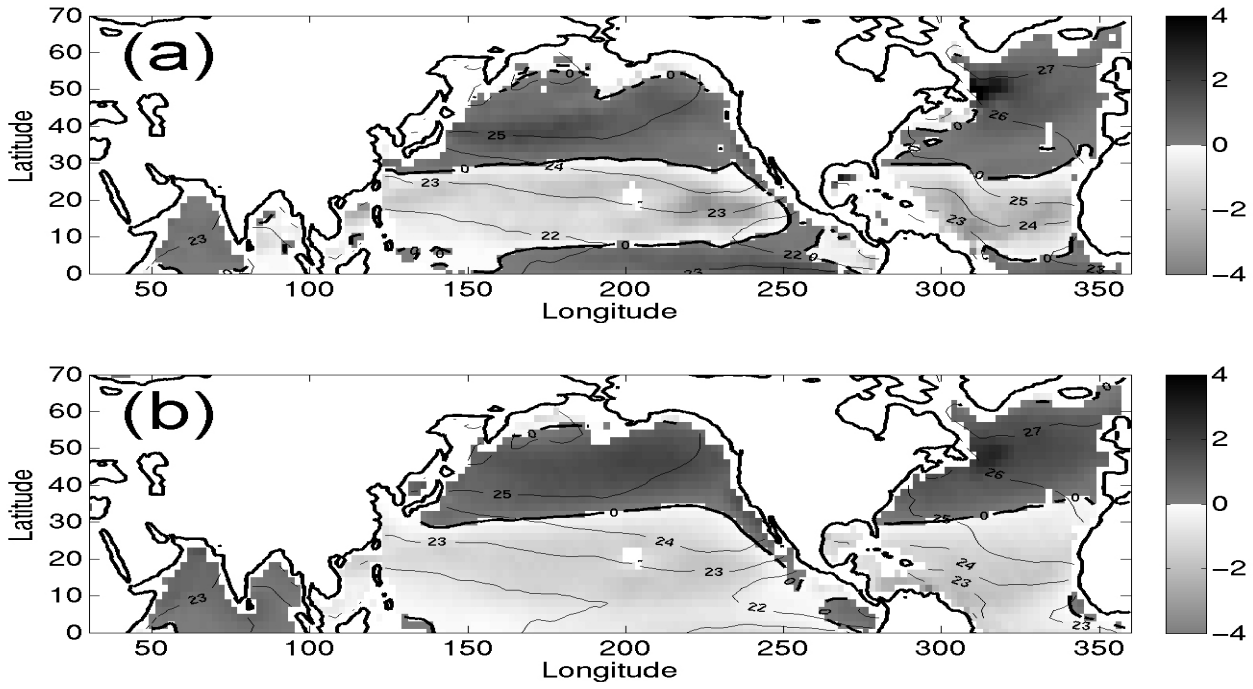
Figure 4: Same as Fig. 3 but by simplifying (12) as (a) $\tau_x(\partial\sigma_m/\partial y)/\rho_o h$ and

(b) $\tau_x(\partial\sigma_m/\partial y)_{ref}/\rho_o h$ in wich $(\partial\sigma_m/\partial y)_{ref} = 1kgm^{-3}/1000km$.
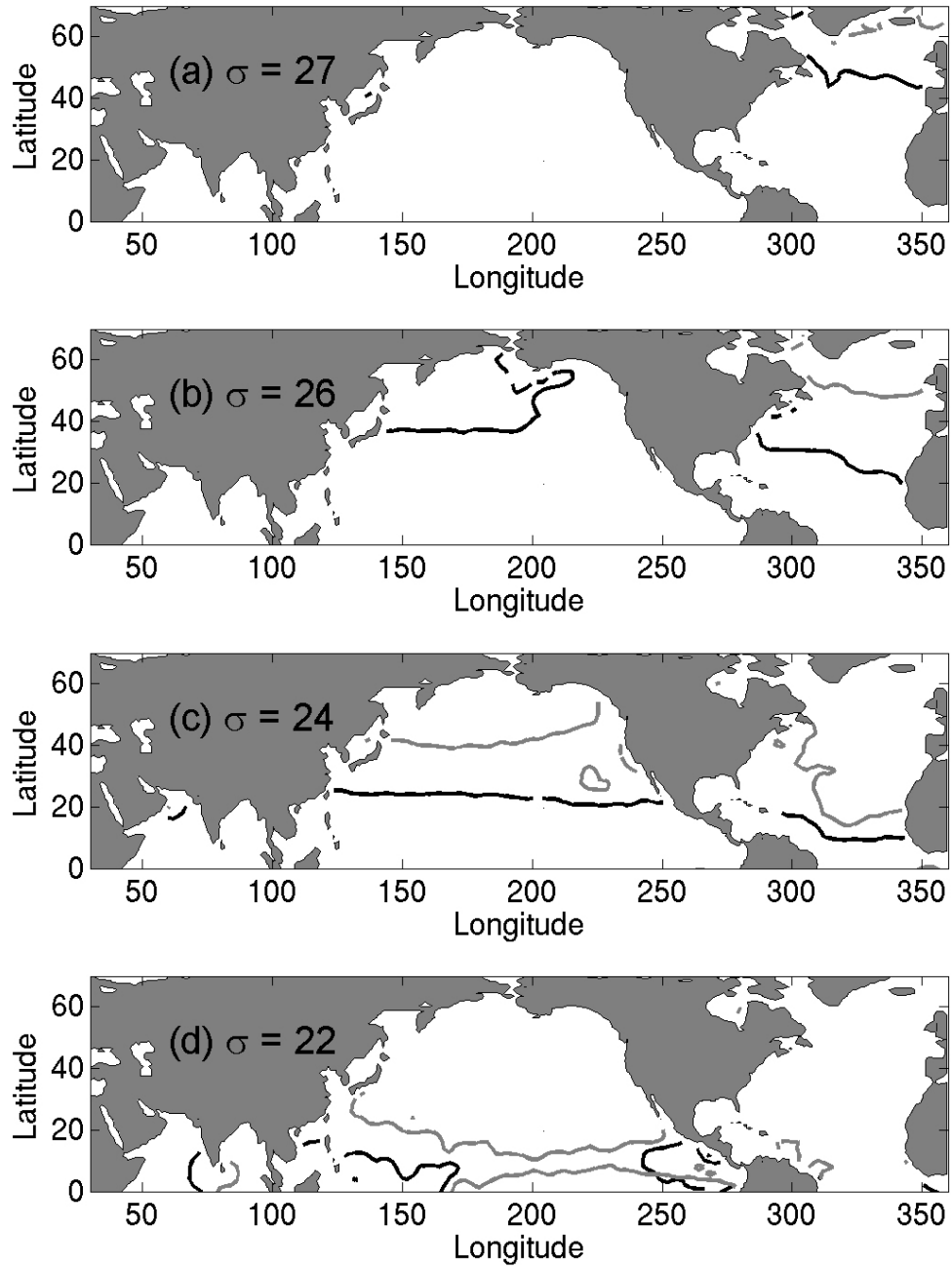
Figure 5: Location of selected mixed layer isopycnal outcrops for March (black) and September (grey). (a) $\sigma_m = 27$ (b) $\sigma_m = 26$ (c) $\sigma_m = 24$ (d) $\sigma_m = 22$.
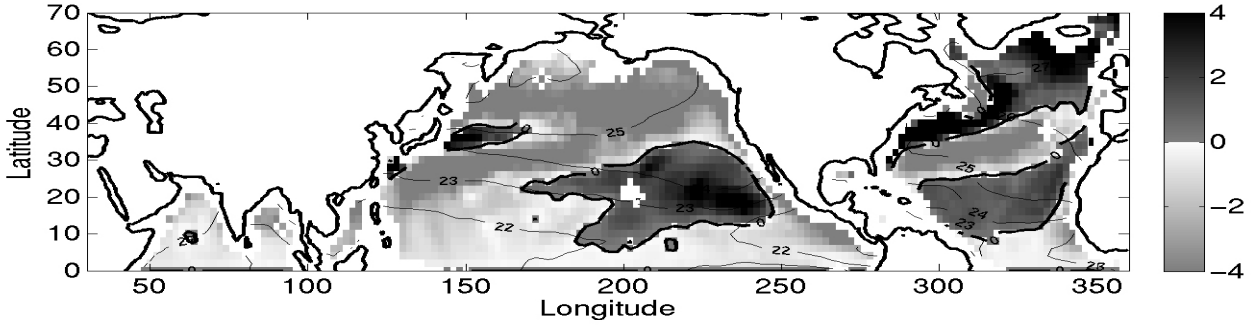
Figure 6: Isopycnal analysis for J_s^{mech}. (a) Monthly Northern Hemisphere PV entry / exit (black when exit, grey when entry, $CI = 5pvs\ s^{-1}\ \Delta\sigma_m^{-1}$) (b) Annual mean of (a) for the North Atlantic (dashed) and North Pacific + Indian (continuous) basins. A positive value indicates PV exit.
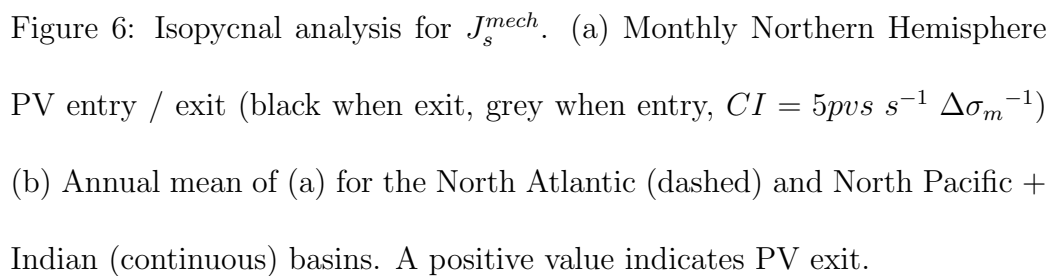
Figure 7: Same as Fig. 3 but for the annual mean diabatic contribution J_s^{diab} (air-sea buoyancy flux + entrainment) to the sea surface PV entry/exit. A value $\Delta_{ent}\sigma = 0.5\ kgm^{-3}$ was used to produce this map.
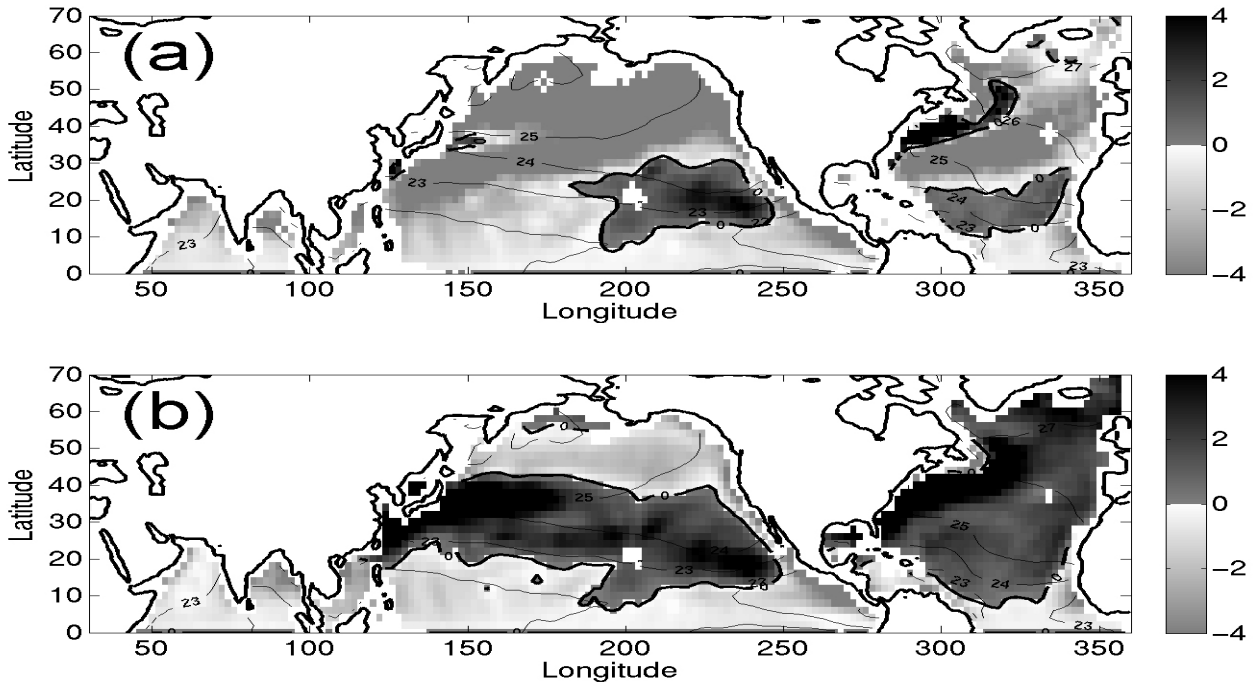
Figure 8: Same as Fig. 7 but with $\Delta_{ent}\sigma = 0$ (a) with the seasonal cycle in mixed layer depth (b) without seasonal cycle in mixed layer depth (i.e., h set to its annual mean value).
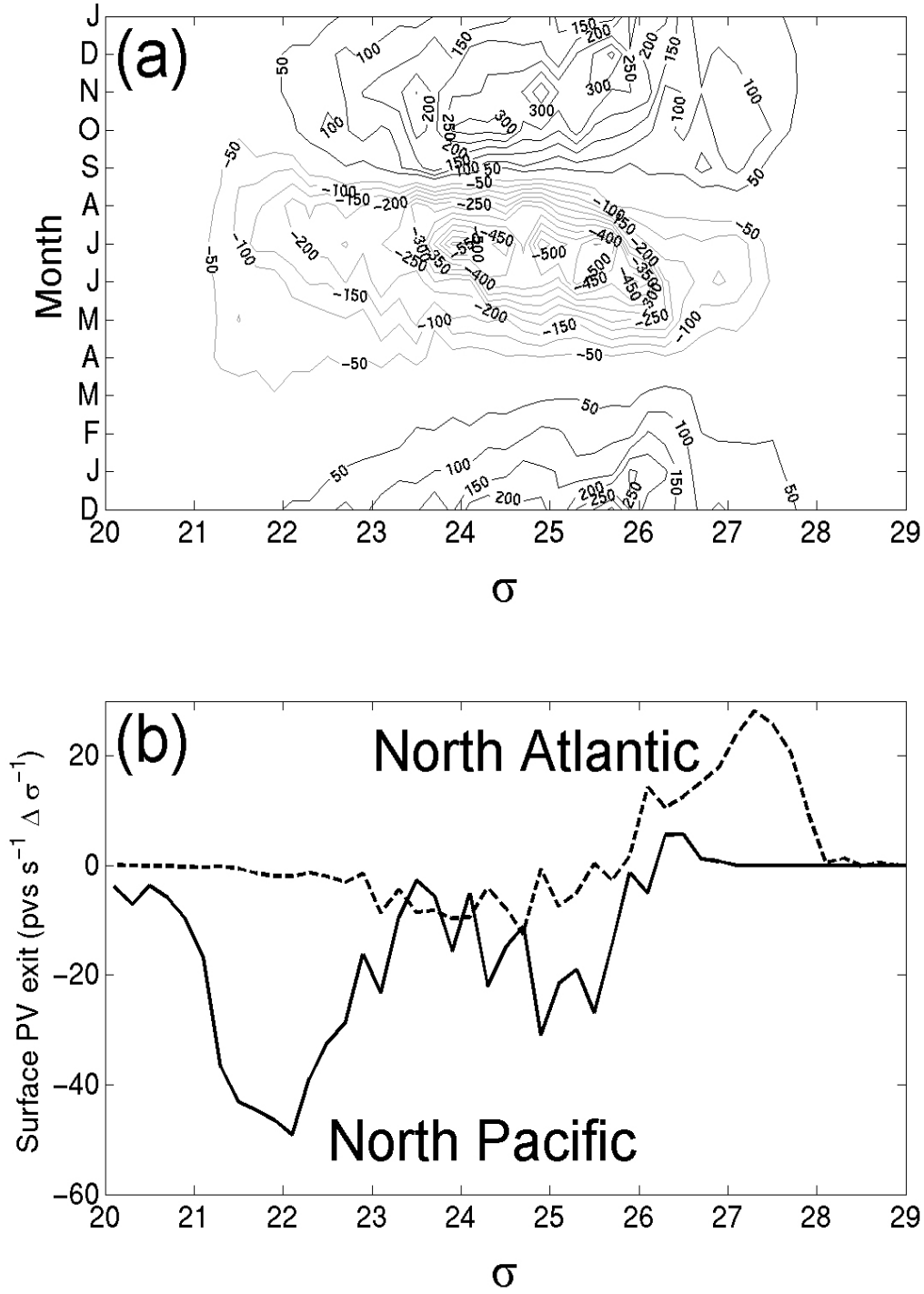
Figure 9: Same as Fig. 6 but for J_s^{diab}. A value $\Delta_{ent}\sigma = 0.5\ kgm^{-3}$ was used in the calculation. Note the large contour interval ($CI = 50\ pvs\ s^{-1}\ \Delta\sigma_m^{-1}$) in (a) compared to Fig. 6a.
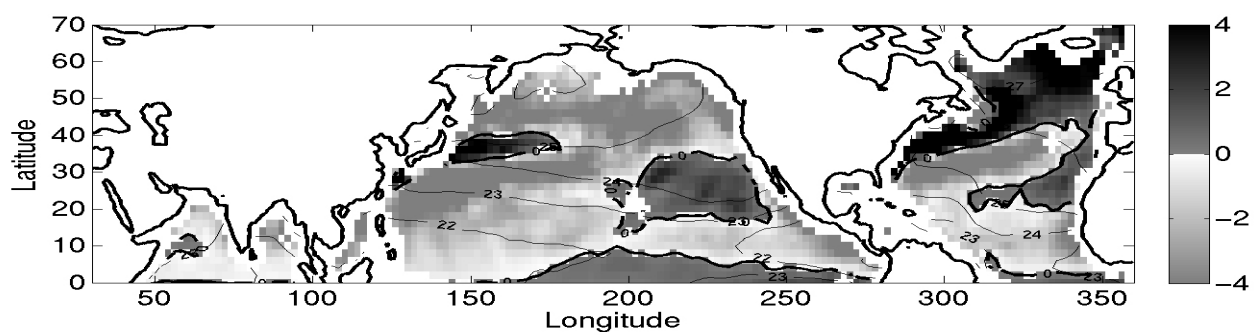
Figure 10: Same as Fig. 3 but for the net PV entry / exit at the sea surface.
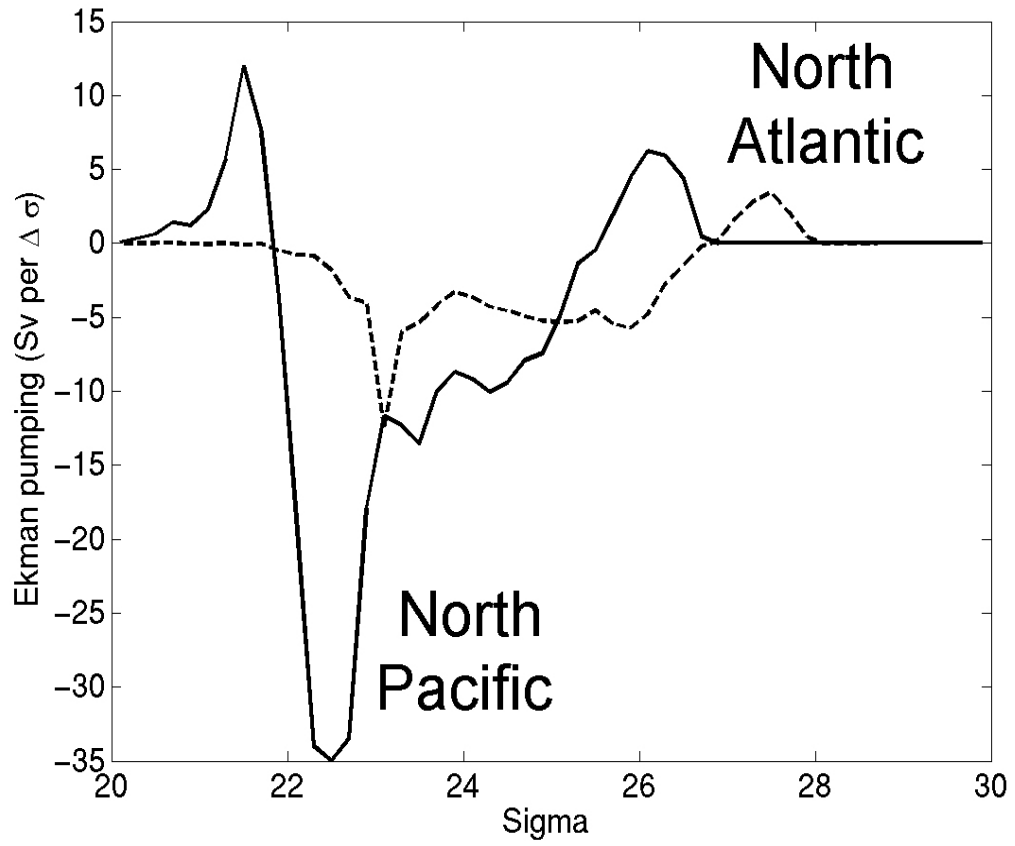
Figure 11: Integrated Ekman pumping w_{Ek} over isopycnal layers of width $\Delta\sigma = 0.2kg\ m^{-3}$, in units of $Sv\Delta\sigma^{-1}$ $(1Sv = 10^6 m^3 s^{-1})$.
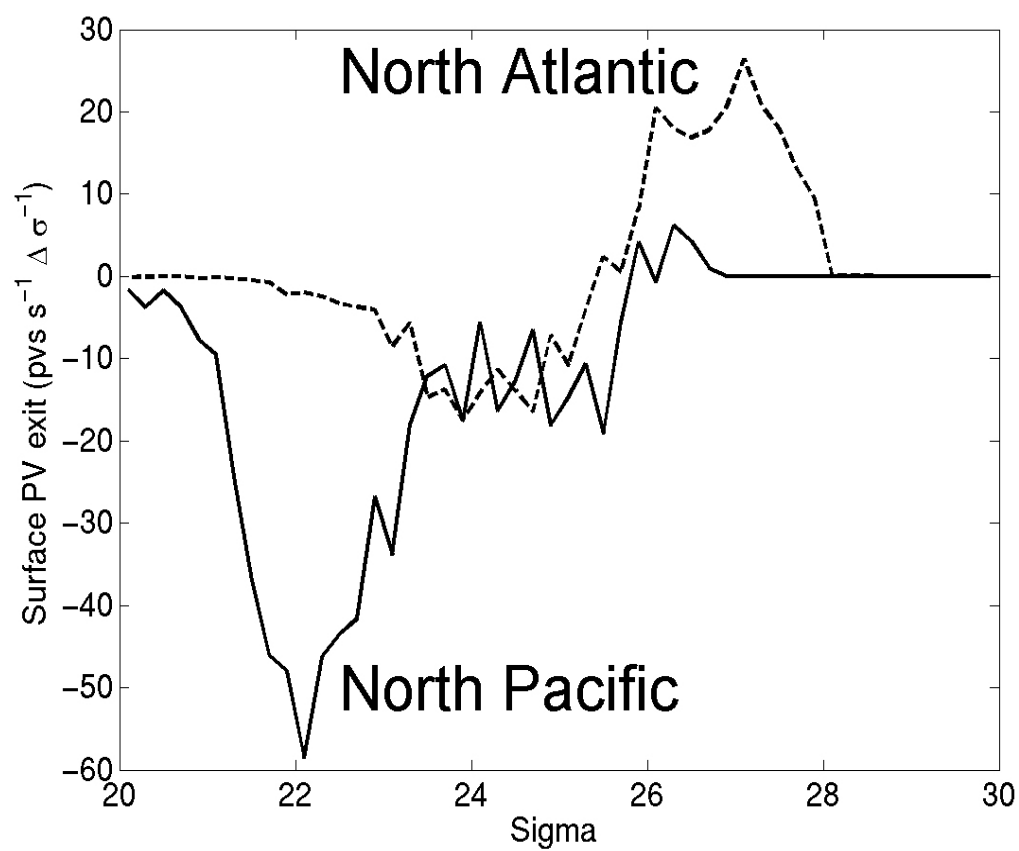
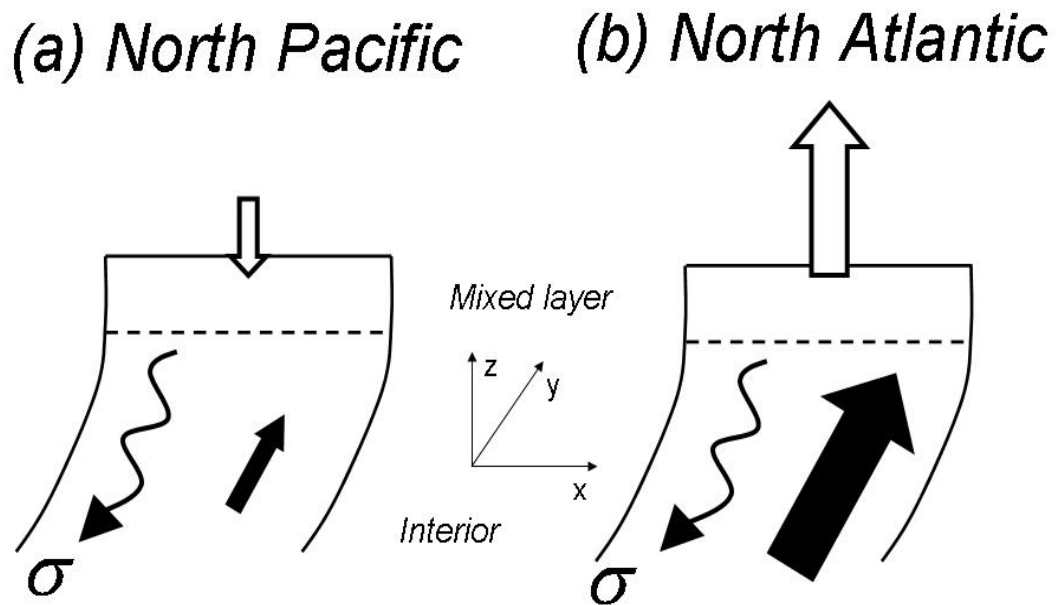Figure 12: Same as Fig. 6b but for the net PV entry / exit at the sea surface.

Figure 13: A schematic of PV transport along a subpolar gyre isopycnal in the North (a) Pacific (b) Atlantic. The entry / exit of PV at the sea surface is indicated by a white arrow, while the advective transport of PV by the mean Sverdrup flow is depicted by a straight black arrow. Wiggly black arrows depict the advective transport of PV due to eddy motions.